Title

Two-photon double ionization of atomic beryllium with ultrashort laser pulses

Journal

Physical Review A, 92(5)

ISSN

2469-9926

Authors

Yip, FL
Palacios, A
Martín, F
et al.

Publication Date

2015-11-01

DOI

10.1103/physreva.92.053404

Peer reviewed

Two-photon double ionization of atomic beryllium with ultrashort laser pulses

F. L. Yip,[1] A. Palacios,[2] F. Martín,[2,3] T. N. Rescigno,[4] and C. W. McCurdy[4,5]

[1]*Department of Science and Mathematics, California Maritime Academy, Vallejo, CA 94590, USA*
[2]*Departamento de Química, Modulo 13, Universidad Autónoma de Madrid, 28049 Madrid, SPAIN*
[3]*Instituto Madrileño de Estudios Avanzados en Nanociencia, Cantoblanco, 28049 Madrid, SPAIN*
[4]*Lawrence Berkeley National Laboratory, Chemical Sciences, Berkeley, California 94720, USA*
[5]*Department of Chemistry, University of California, Davis, CA 95616 USA*

(Dated: October 21, 2014)

We explore the two-photon double ionization of beryllium induced by ultrashort pulses. We use a time-depedent formalism to evaluate the ionization amplitudes and generalized cross sections for the ejection of the $2s^2$ valence shell of atomic beryllium in the presence of a fully-occupied $1s^2$ core shell. The similar symmetry of the overall process in two-photon double ionization permits a direct comparison between our results for Be and previous work on He atom in [1], revealing details about the nature of electron correlation within these two atoms manifested in the continuum electron dynamics. We explore the contributions from direct and sequential double ionization of beryllium. Different from the helium-like process, the sequential double ionization process reveals a dominant pathway via excitation ionization through the $Be^+(2p)$, which strongly determine the profiles and pulse-duration dependencies of the energy and angle differential cross sections.

I. INTRODUCTION

Investigations of the interaction of atoms and molecules with ultrashort laser pulses has grown dramatically since experimental methods have advanced the production on nonlinear optical sources with high intensities [2–6]. More specifically, a complete understanding of double ionization processes of atomic targets by absorption of one or few XUV photons has been the subject of many theoretical works in the last years and has often advanced experimental work in this field. Because both electrons are simultaneously ejected into the continua, these studies are expected to shed light on the role and importance of electron correlation in atoms. The simplest system for such study, atomic helium, has seen the contribution of many theoretical treatments (see [7] and references therein) to elucidate the first experiments conducted with free electron laser sources (FELs) [8] and high-harmonic generation (HHG) [9, 10]. Beyond helium and other purely two-electron targets, however, the increasing demands of accurately representing more complicated atomic targets grows as additional electrons must be appropriately accounted for. Very few reliable *ab initio* theoretical works for multielectron targets are available for one-photon double ionization of atoms like Be or Mg [11–13], and there are even scarcer the studies for double ionization upon two photon absorption [14]. From an experimental point of view, two-photon double ionization processes bring the challenge of measuring a minor contribution with respect to the also present single ionization channel. Therefore, it implies the necessity of coincident measurements of electrons and ions to unravel the different energetically-open processes. Moreover, two-photon experiments require a coherent light source in the XUV region involving techniques that control the polarization, wavelength, phase and intensity of the pulse. Such challenges have been overcome by a few experimental works and two-photon double ionization measurements are now available for neon using FEL light [15] or in Kr or Ar [16] and more recently in xenon [17] using HHG techniques to explore the autoionizing intermediate states. Towards better understanding the multi-electron dynamics of these more complicated atomic targets, we seek to explore the two-photon double ionization of Be induced by ultrashort pulses with durations shorter than a few fs. We present results for different energies and angles for the emitted electrons, and discuss the information that can be retrieved from these differential quantities.

Our goal is also making connection with the previous body of work investigating helium in order to elucidate the fundamental role of electron correlation for atoms that share a similar electron configuration, and therefore, represent the same initial and final state symmetry undergoing a two-photon absorption. Aside from the similar consequences of the initial state ^1S symmetry of both targets and selection rules which make this a natural analogue of the more well-studied helium, the inherent energetics of double photoionization of the valence electrons of beryllium is expected to have profound consequences on the *mechanism* of double photoejection relative to helium. In particular, the role of sequential ionization (where the first photon singly ionizes the neutral beryllium and the second photon ejects the second electron from the intermediate cation) is energetically open much closer to the double ionization threshold where a non-sequential (direct) absorption of the two photons is the only means to the double continuum. The consequences of non-sequential vs. sequential ionization have been well-studied in helium with focus on the role of electron correlation, for which it is absolutely necessary to describe accurately the correlated dynamics for the former but less important in the latter. For beryllium, substantially less analysis of the non-sequential and sequential mechanisms has been previously reported [14]. We thus include a complete study of such mechanisms with

specific interest on the pulse duration effects. Together with accurate theoretical calculations we discuss the suitability of simple models to reproduce some important features appearing in the two-photon double ionization observables.

In the first section, we review the theoretical method and relevant computational details for the specific case of two-photon double ionization on frozen-core multielectron targets. In section III, we discuss the differences in the role of non-sequential and sequential ionization mechanisms compared to helium, as well as how beryllium provides some unique features that can further elucidate how electron correlation impacts the apparent cross sections discussed in greater detail in section III A and section III B. Brief conclusions follows in section IV.

II. THEORY

A time-dependent treatment is required to explore the two-photon double ionization of beryllium induced by ultrashort pulses. The methodology here employed combines an accurate description of the multielectron wave-function, as introduced in our previous works for time-independent problems on lithium and beryllium [18, 19], with the time-dependent approach and the exterior complex scaling (ECS)-based amplitude extraction method both initially developed for helium and detailed in Refs. [20, 21]. This time-dependent formalism for frozen-core multielectron targets has been recently used to successfully describe the one-photon single and double ionization of Be in [22], where we found a good agreement with previous theoretical results and experimental data available. In the following, we give a highlight of the four-electron target representation and focus on the relevant details in the implementation to take into account the action of the ultrashort pulse.

A. Time-dependent four-electron wave-function

The interaction of a finite pulse with the atomic target is described by solving the time-dependent Schrödinger equation (TDSE)

$$i\frac{\partial}{\partial t}\Psi(t) = H(t)\Psi(t), \tag{1}$$

where $H(t) = H + V(\mathbf{r}, t)$ is the full Hamiltonian (Eq. 4) for the beryllium valence electrons plus the interaction term with the field $V(\mathbf{r}, t)$. Employing the dipole approximation in the length gauge, we describe the laser-atom interaction by $V(\mathbf{r}, t) = \mathbf{E}(t) \cdot \mathbf{r}$, where the time-varying electric field $\mathbf{E}(t)$ for a short pulse with duration T is

$$\mathbf{E}(t) = \begin{cases} E_0 F(t) \sin(\omega t)\hat{\epsilon}, & 0 \le t \le T \\ 0, & \text{otherwise} \end{cases} \tag{2}$$

where ω and E_0 are the central frequency and the maximum electric field amplitude of the pulse, respectively. We have chosen a sine-squared envelope, $F(t) = \sin^2(\pi t/T)$, to account for a finite pulse length of T with a smooth switch-on/switch-off of the field.

We write the four-electron wave-function explicitly, which is essentially different from previous theoretical works performed on double ionization of beryllium where the $1s^2$ core is treated using model potentials or pseudopotentials [14, 23]. In our description, the wave function for the four electrons of beryllium is expanded as

$$\Psi(t) = \sum_{i,j} C_{i,j}(t) \left| \xi_i(r_1) Y_{l_i}^{m_i}(\Omega_1)\, \xi_j(r_2) Y_{l_j}^{m_j}(\Omega_2) \varphi_{1s}(3)\, \varphi_{1s}(4) \right| \tag{3}$$

where the inner-shell $1s^2$ electrons are held fixed in the expansion configurations (i.e., frozen-core approximation), and consequently the expansion coefficients will only depend on the valence $2s^2$ electrons that will be ionized into the continuum. This description is valid because of the large energetic separation between the valence and core electrons and their role can be described by a closed-shell interaction potential. Thus, the relevant Hamiltonian for the valence electrons becomes (in atomic units)

$$H = h(1) + h(2) + \frac{1}{r_{12}} + E_{\text{core}}, \tag{4}$$

where $1/r_{12}$ is the repulsion of valence electrons and the impact of the static $1s^2$ core is accounted for in each one-body operator h,

$$h = T - \frac{Z}{r} + 2J_{1s} - K_{1s}, \tag{5}$$

where T is the one-electron kinetic energy, the nuclear attraction is $-Z/r$ with a nuclear charge $Z = 4$, and $2J_{1s}$ and K_{1s} are the direct and exchange interactions of each valence electron with the $1s^2$ core, respectively. Because each determinant in Eq. 3 contains the same $1s$ orbital, the last term in Eq. 4 accounts for the energetic contribution of $1s^2$ core,

$$E_{\text{core}} = 2\epsilon_{1s} + J_{1s}, \tag{6}$$

where ϵ_{1s} is the orbital energy of each $1s$ electron. Since our focus is on the valence electrons, the constant core energy is factored off and the zero-point for the double ionization energy in what follows is referenced to the ionized electrons infinitely separated from the Be^{2+} residual dication.

In order to construct the wave function with occupied inner-shell orbitals as in Eq. 3 and maintain a computationally efficient and flexible description of the ionized electron dynamics at distances far beyond the nuclei, we employ a discrete variable representation with finite elements (FEM-DVR) [24] radial basis for all electrons.

This requires the construction of a number of atomic orbitals out of the underlying FEM-DVR radial basis,

$$\xi_\alpha(r) = \sum_{j=1}^{M} U_{\alpha j}\chi_j(r), \tag{7}$$

where the radial atomic orbital basis $\xi_\alpha(r)$ is expanded in the FEM-DVR radial functions $\chi_j(r)$ via the unitary transformation matrix $U_{\alpha j}$. Since the occupied atomic orbitals have limited extent, we rely on the the finite element nature of the underlying radial basis to only reconstruct the orbitals in Eq. 7 over the innermost regions near the nuclei, i.e. over the radial extent of the $1s$ orbital. Beyond that region, and in particular over the radial distances necessary to describe ionization processes, the primitive FEM-DVR basis is untransformed. The main advantage here is that local potentials, particularly, the two-electron repulsion, retains its diagonal radial representation over large portions of the radial space. This framework accommodates an efficient description of the radial coordinates of the outgoing electrons while permitting a limited number of atomic orbitals to describe the core interactions with those electrons held fixed in the expansion determinants of Eq. 3.

Our representation of the inner-shell atomic orbitals on a double ionization grid provides an appropriate balance to accurately represent the core direct and exchange potentials that the outgoing electrons experience while maintaining flexibility and efficiency in describing the long-range dynamics far from the nuclei. It is worth remarking that, after solving the TDSE, the extraction of double ionization amplitudes from the propagated wave-function $\Psi(t)$ in Eq. 3 requires the use of the same frozen-core potentials to remove accessible single ionization components at a particular final-state total energy E. In the following, we review the formalism employed to extract those amplitudes and to define the generalized cross sections for the specific problem of two-photon double ionization.

B. Two-photon double ionization amplitudes

Beyond the end of the pulse, the time evolution of the wave function, $\Psi(t > T)$, is governed only by the field-free Hamiltonian H of Eq. 4. To extract any spectral information, we first need the asymptotic form of the wave packet, i.e. to carry out an implicit integration from $t = T$ through $t = \infty$ and, then, a Fourier transform to obtain the scattering function at a given final energy, E. As previously demonstrated in Refs. [20, 21], instead of performing a numerical integration, one can formally compute the scattering function for electrons ejected at a given total energy E by solving the time-independent Schrödinger equation using as the initial condition the time-propagated wave function, $\Psi(t \geq T)$. Therefore, the problem can be written as the following driven equation:

$$(E - H)\Psi^{+}_{\rm sc}(\mathbf{r}_1, \mathbf{r}_2) = \Psi(\mathbf{r}_1, \mathbf{r}_2, T), \tag{8}$$

where the time-propagated wave packet contains the information on all significantly populated spectral components from the action of the ultrashort pulse. This wave packet can then be formally decomposed as

$$\begin{aligned}
&\Psi(\mathbf{r}_1, \mathbf{r}_2, t > T) = \\
&\psi_{\rm bound}(\mathbf{r}_1, \mathbf{r}_2, t) + \psi_{\rm single}(\mathbf{r}_1, \mathbf{r}_2, t) + \psi_{\rm double}(\mathbf{r}_1, \mathbf{r}_2, t) = \\
&\psi_{\rm bound}(\mathbf{r}_1, \mathbf{r}_2, t) + \sum_n \int d^3\mathbf{k}_n \; C(\mathbf{k}_n)\psi^{-}_{\mathbf{k}_n}(\mathbf{r}_1, \mathbf{r}_2) \\
&\quad + \iint d^3\mathbf{k}_1 d^3\mathbf{k}_2 \; C(\mathbf{k}_1, \mathbf{k}_2)\psi^{-}_{\mathbf{k}_1,\mathbf{k}_2}(\mathbf{r}_1, \mathbf{r}_2).
\end{aligned} \tag{9}$$

The solution of the driven equation in Eq. 8 extracts the information for the given energy E from all components (bound, single and double ionization components). Because we are interested in the ionization components, we will use exterior complex scaling (ECS) to enforce the correct outgoing-wave boundary conditions for $\Psi^{+}_{\rm sc}(\mathbf{r}_1, \mathbf{r}_2)$ (see Ref. [25] for details). Solving the driven equation with ECS extracts the second and third terms in the formal expansion of Eq. 9 at total energy E. Once we have identified the amplitudes in the asymptotic form of the scattering wave, we can separately compute them for double (or single) ionization, by employing a well-tested formalism that reduces the problem to the solution of a simple surface integral [20, 25]. The double ionization amplitude $C(\mathbf{k}_1, \mathbf{k}_2)$ for ejecting two valence electrons with momenta $\mathbf{k}_1$ and $\mathbf{k}_2$ and yielding the frozen-core Be^{++} dication, is thus given by

$$\begin{aligned}
C(\mathbf{k}_1, \mathbf{k}_2) = \frac{1}{2}e^{i\gamma} \int \big\{ &\phi^{-*}_{\mathbf{k}_1}(\mathbf{r}_1)\phi^{-*}_{\mathbf{k}_2}(\mathbf{r}_2)\nabla\Psi^{+}_{\rm sc}(\mathbf{r}_1, \mathbf{r}_2) \\
&- \Psi^{+}_{\rm sc}(\mathbf{r}_1, \mathbf{r}_2)\nabla[\phi^{-*}_{\mathbf{k}_1}(\mathbf{r}_1)\phi^{-*}_{\mathbf{k}_2}(\mathbf{r}_2)]\big\} \cdot d\mathbf{S},
\end{aligned} \tag{10}$$

where we need to carefully chose the appropriate testing functions, $\phi^{-*}_{\mathbf{k}_1}(\mathbf{r}_1)\phi^{-*}_{\mathbf{k}_2}(\mathbf{r}_2)$, that eliminate all other components in Eq. 9 by orthogonality [20, 25, 26]. The individual testing functions $\phi^{-}_{\mathbf{k}}(\mathbf{r})$ represents a continuum solution of the one-body Hamiltonian in Eq. 5 that asymptotically sees a nuclear charge of $Z = 2$. Thus, the other role of properly accounting for the frozen-core $1s^2$ electrons is to perfectly screen the bare nuclear charge of beryllium at long distance to account for the the residual charge seen by the outgoing electron(s). Note that the γ in Eq. 10 is a volume-dependent phase that imparts no physical consequences [26].

C. Generalized differential cross sections

We employ time-dependent perturbation theory (TDPT) to define double ionization amplitudes. The propagated wave packet, after the interaction with a single pulse, is utilized to extract double ionization amplitudes over an *energy range* consistent with the bandwidth

of the pulse centered on ω. Regardless the final channel, single or double ionized continua, one can use the first-order TDPT expressions to exactly write the one-photon absorption amplitudes as a product of the dipole matrix element from the initial to the final state and a "shape function" which is merely the Fourier transform of the pulsed radiation [20, 27]. An equivalent treatment is here used for the two-photon absorption. Although the factorability of the transition amplitude is no longer strictly exact, it remains valid in the absence of resonant states with the one-photon transition [21].

The generalized cross section differential in both angle and electron ejection for a two-photon absorption process is defined as the transition rate M_{if} from an initial state i to a final state f, which is given by the Fermi's golden rule, divided by the photon flux. In the length gauge, the differential cross section is written as

$$\frac{\partial\sigma}{\partial\Omega\partial E_1^f\partial E_2^f} = \frac{8\pi^2 k_1 k_2 (\omega_{fi}/2)^2}{c^2}|M_{if}|^2 \tag{11}$$

where the transition rate involves a summation over all the eigenstates of the target:

$$M_{if} = \sum_m \langle\Phi_f^-|\boldsymbol{\epsilon}\cdot\mathbf{p}|\Phi_m\rangle\langle\Phi_m|\boldsymbol{\epsilon}\cdot\mathbf{p}|\Phi_i\rangle. \tag{12}$$

Furthermore, the integral of Eq. 11 over the directions of the ejected electrons yields the single differential (energy sharing) generalized cross section.

The two-photon absorption amplitude is written in second-order TDPT as

$$C^{2\omega} = \left(\frac{-i\alpha E_0}{em}\right)^2 \sum_m \langle\Phi_f^-|\boldsymbol{\epsilon}\cdot\mathbf{p}|\Phi_m\rangle\langle\Phi_m|\boldsymbol{\epsilon}\cdot\mathbf{p}|\Phi_i\rangle F^{2\omega}(\omega,\omega_{fi},\omega_m,T) \tag{13}$$

where $F^{2\omega}$ is the Fourier transform of the pulse at each transition, thus implying a double integral with an explicit m-state dependence. Nevertheless, we found that this function can be reasonably approximated to an m-independent analytical form, $\mathfrak{F}(\omega,\omega_{fi},T)$, which becomes exact in the long time limit ($T\to\infty$) provided no intermediate state resonances lie within the bandwidth of the pulse (further details are given in [20]). Consequently, this approximation allows for the factorability of the time-dependent function in expression Eq. 13, and allows us to rewrite the generalized two-photon double ionization cross section as

$$\frac{d\sigma^{2\omega}}{dE_1 d\Omega_1 d\Omega_2} = \frac{8\pi^2 k_1 k_2 (\omega_{fi}/2)^2}{c^2|E_0|^4}\frac{|C(\mathbf{k}_1,\mathbf{k}_2)|^2}{|\mathfrak{F}(\omega,\omega_{fi},T)|^2}, \tag{14}$$

where the approximated double integral for the Fourier transform gives what has previously been referred to as the "shape function":

$$\mathfrak{F}(\omega,\omega_{fi},T) = \frac{6e^{-iT(2\omega-\omega_{fi})}\left(e^{iT(2\omega-\omega_{fi})}-1\right)\pi^4}{(2\omega-\omega_{fi})\left[T^4(2\omega-\omega_{fi})^4 - 20\pi^2T^2(2\omega-\omega_{fi})^2 + 64\pi^2\right]}. \tag{15}$$

The sequential ionization process, in which one photon first ionizes the neutral target and the second photon ionizes the ion, implies two separate transition rates, and therefore is not appropriately described by a cross section as in Eq. 11. In fact, this expression would become singular at the energies that are resonant with each ionization threshold of the neutral. Nevertheless, the (generalized) formulas given here are still well-defined and maintain their connection to the non-sequential ionization threshold where the two-photon cross section is physical below these intermediate-state resonances. In addition, the generalized cross sections continue to be proportional to moduli-squared double ionization amplitudes in Eq. 14. For convenience, we thus will use these expressions to define the cross section at any frequency to elucidate the role of the pulse length and other pulse-dependent consequences on the double ionization amplitudes.

D. Computational implementation

The valence and core electrons for beryllium in Eq. 3 are expressed radially in the orbital-DVR basis while the angular coordinates of the valence electrons are expanded in coupled spherical harmonics, $\mathcal{Y}_{l_1,l_2}^{L,M}(\hat{\mathbf{r}}_1,\hat{\mathbf{r}}_2)$, best suited for the spherical atomic symmetry. The first two finite elements from the origin, with boundaries at 2.0 bohr and 7.0 bohr are used to construct the atomic orbitals. Beyond that, the radial coordinate of the the valence electrons is described by the primitive FEM-DVR with 17th order in finite elements of length 8.0 bohr. The initial bound state is found by diagonalizing the field-free Hamiltonian on a grid with radial extent up to $R=44.0$ bohr. The diagonalization is performed by using the eigenvalue problem solvers implemented in the SLEPc libraries [28, 29]. The time propagation of the pulse from zero up to $t=T$ proceeds on a larger radial grid up to 180.0 bohr. To solve the driven equation we use an ECS contour rotated at R_0 is 180.0 bohr with two additional complex scaled elements appended with boundaries at 188.0 and 220.0 bohr. In comparison to helium, larger grid extents are necessary to converge the generalized cross sections, reflecting the lower ionization threshold and larger $2s^2$ valence shell of beryllium. The TDSE was solved using a Cranck-Nicholson propagation scheme with time-steps in the range of 0.25-3 fs. For each time step in the propagation, as well as for the driven equation that defines the scattering function, we solve a system of linear equations using the Krylov solvers implemented in the PETSc libraries [30]. The pulses here employed have an intensity of 10^{12} W/cm^2, which is low enough to ensure the suitability of the TDPT expressions.

In comparison to our previous time-dependent treatment of the single photon double ionization of beryllium, the number of one-electron angular terms that must be included is much larger. The generalized TDCS appeared converged with up to $l_{\max}=11$ used for each electron, substantially larger than one-photon beryllium

double ionization and the two-photon double ionization of helium. This reflects the larger contribution of angular correlation in beryllium compared to helium and the accessibility of higher individual electron partial waves as more photons are absorbed. However, the total angular momentum transition from the similarly described ^1S ground state symmetry for both helium and beryllium is the same; two-photon absorption places the ionized wave function in the ^1S and ^1D continua in the dipole approximation.

III. TWO-PHOTON DOUBLE IONIZATION OF BE

In what follows, we compute energy and angular differential generalized cross sections for two-photon double ionization of the outer shell in Be. We compare these results with the trends and behavior observed for the same processes in the helium atom (more specifically those in [7] and references therein), in order to explore the role of the "spectator" $1s^2$ core and the relevance of the different electron correlation terms in the double ionization process. Moreover, we carry out calculations with different pulse lengths to elucidate the intrinsic time scales associated with the signatures of the sequential electron ejection.

The first part of the present section is devoted to introduce the energy diagrams of Be and analyze the energy differential cross sections for different pulse durations. The energetics associated to the 2s electrons in the presence of the $1s^2$ core differs significantly from the 1s electrons in helium, consequently modifying the profiles in the cross sections differential in the electron energies.

In the second part of this section, we discuss the role and signature of electron correlation, which clearly manifests in the angular distributions as demonstrated in [21], i.e. in the generalized cross sections differential in the angle of electron ejection for a given energy.

A. Generalized cross sections *versus* energy sharing

The energy diagram of beryllium is shown in Fig. 1. From the ground state energy of $E_0 = -27.42$ eV of the $2s^2$ valence electrons calculated for Be, two-photon double ionization is accessible for photon energies of $\hbar\omega = 13.71$ eV. In contrast with helium, the energy range to observe a pure non-sequential (direct) double ionization by two photons of beryllium is very small. In fact, for energies of 14.14 eV, it is already possible to eject both electrons into the continua by first ejecting an electron from the neutral atom and leaving the ion in its excited state ($[1s^2]2p\ ^2P^o$). Therefore, there is a narrow window of 0.45 eV (14.14-13.71 eV) were direct double ionization will take place alone. This implies that the large bandwidths associated to ultrashort pulses (for instance, a pulse length of T=1 fs has a full-width at half maximum in energy of $\simeq 6$ eV) will always capture both the direct and the sequential components for two-photon double ionization. We omit any discussion of total ionization cross sections, because they are only well-defined in this very narrow non-sequential region. This is not the case for helium atom, where there is an energy difference of $\simeq$15 eV (54.4 - 39.5) eV, between the two-photon double ionization potential at 39.5 and the 54.4 eV energy at which the sequential process opens.

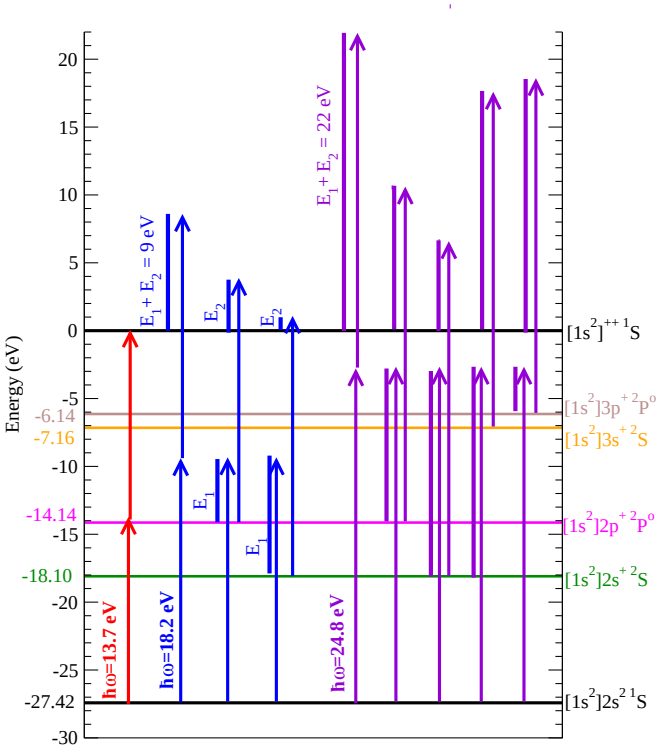

FIG. 1: (Color online) Energy level diagram of the frozen-core beryllium atom. The ground state energy of the valence electrons is $E_0 = -27.42$ eV. Non-sequential ionization (red leftmost arrows) becomes the first pathway to the double continuum for $\hbar\omega = 13.71$ eV photons. Sequential ionization via the first energetically open channel occurs for photons with energy above 14.14 eV and proceeds via the $Be^+(2p)$ intermediate cation. For photons above 18.10 eV, the second sequential pathway is accessible via the $Be^+(2s)$ intermediate. The central blue arrows and rightmost violet arrows indicate the photon processes considered at two energies as described below.

Another interesting difference with He is the fact that sequential ionization of beryllium first proceeds through an excited state of the ion, i.e., two-photon double ionization through excitation-ionization opens at lower energies (at 14.14 eV) than two-photon double ionization through the ground state of the ion (at 18.10 eV). The opposite situation is found in He. We could then infer that electron correlation is expected to be more meaningful in beryllium relative to helium in the sequential region because the first photoabsorption must move both electrons, one into the continuum and one into the ex-

cited $2p$ orbital of the intermediate cation. Stated in an alternative way, the correlating configuration $2p^2$ of neutral beryllium represents a much more significant contribution to the full configuration interaction expansion of the wave function than it does in helium. Thus we can anticipate the sequential ionization of beryllium will reflect the importance of higher angular momenta correlating configurations in the sequential region with those processes identified by this intermediate state resonance. The beryllium sequential ionization process that is more comparable to the dominant sequential one for helium becomes accessible at slightly higher photon energy. As we previously commented, at $\hbar\omega = 18.1$, the second sequential threshold becomes open and proceeds via the intermediate that leaves remaining valence electron of the cation Be^+ in its ground state $2s$ configuration (see Fig. 1).

We next explore the anticipated signatures of sequential double ionization in the singly differential (generalized) cross section (SDCS), which shows the variation of the double ionization amplitudes with respect to the energy sharing between the two ionized electrons. Note that we choose to plot the SDCS as a function of energy sharing for a fixed total final energy ($E = E_1 + E_2$), instead of fixing the energy of one of the electrons and plot the SDCS as a function of the energy of the second one. The latter would led to assymetric profiles, while we obtain SDCS that are symmetric functions respect to 50% energy sharing, better reflecting the fact that both ejected electrons are indistinguishable. Regardless of the atomic target under study, for an infinite long pulse the sequential process is expected to manifest in the SDCS as singularities centered at the excess energies of each electron [31]. When using finite pulses those peaks will broaden together with the energy bandwidth of the pulse, and for very short pulses the sequential peaks are observed to completely wash out [1]. The disappearance of the sequential peaks can be related to the Fourier broadening of the pulse or to the time required for the sequential process to take place. Only a further analysis of the angular distributions can confirm its origin.

In examining the SDCS we chose two different central energies for the ultrashort pulses: i) 18.2 eV, for which sequential ionization through the ground state of the ion already opens (central blue arrows of Fig. 1) and ii) 24.8 eV, for which sequential ionization through the ground and higher excited states of the ion are also open (rightmost violet arrows in Fig. 1). We investigate the effect of modifying the pulse duration and discuss the time scales observed with respect to the analogous study on helium. Fig. 2 displays the two-photon generalized cross section of beryllium (in units of $\mathrm{cm}^4\ \mathrm{s\ eV}^{-1}$) extracted for a pulse centered at $\hbar\omega = 18.2$ eV, i.e. leaving a fixed excess total energy of $E = 9.0$ eV for the electrons to carry away. The lower x-axis is labeled with the energy sharing and the corresponding absolute energy E_1 of the electron is shown on the upper x-axis.

The effect of increasing the pulse length results in an

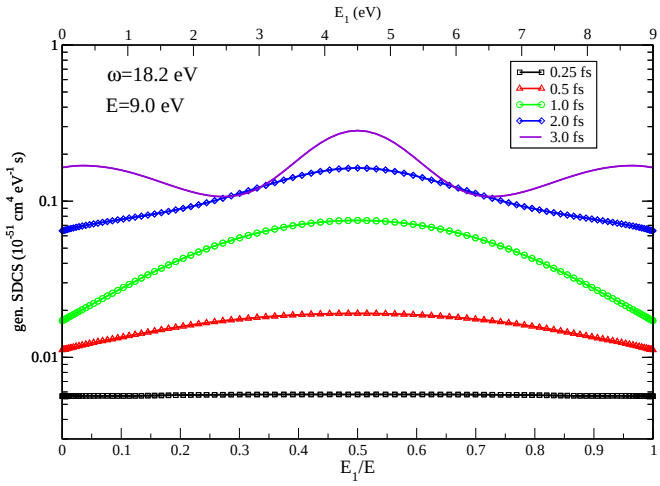

FIG. 2: (Color online) Generalized energy sharing cross section (SDCS) for two-photon double ionization of Be with $\hbar\omega = 18.2$ eV photons for various pulse durations. The excess energy above the double ionization threshold is $E = 9.0$ eV. A pair of sequential peaks near equal energy sharing $E_1/E = 0.5$ via the excited $Be^+(2p)$ intermediate is unresolved by these bandwidth-limited pulses. Longer pulses do begin to resolve the signature of helium-like sequential ionization appearing at extreme energy sharings.

increase of the magnitude of the ionization amplitudes, as well as an enhanced resolution of the signatures of the sequential process peaks. In principle, we would expect to observe two pairs of peaks [7], one pair associated with the sequential process via the $Be^+(2p)$ and the other pair with the sequential process via the $Be^+(2s)$; i.e, electrons ejected at $E_1 = E_0 - \epsilon_{2p} + \hbar\omega$=4.92 eV and $E_2 = \epsilon_{2p} + \hbar\omega = 4.06$ eV for the first pair of peaks and electrons ejected at $E_1' = E_0 - \epsilon_{2s} + \hbar\omega$ =8.88 eV and $E_2' = \epsilon_{2s} + \hbar\omega = 0.1$ eV for the second pair. However, these signatures actually appear smoothed out, since we are using ultrashort pulses. Moreover, because the energy level of the first energetically open excitation ionization resonance via the $Be^+(2p)$ lies almost exactly halfway between the ground state energy E_0 of the valence electrons and the double ionization threshold, the pair of sequential ionization peaks that first appear corresponding to energies E_1 and E_2 are separated by $E_0 - 2\epsilon_{2p} = 0.86$ eV. The consequences of this energy level spacing places the pair of sequential peaks separated by less than 1 eV, a spacing smaller than the energy bandwidth of the longest few-femtosecond pulse considered here. In fact, the first pair of expected peaks becomes a single central peak in the SDCS in Fig. 2 because the broad energy bandwidth of these ultrashort pulses does not resolve the 0.86 eV energy gap (4.92-4.06 eV) between them. Only pulse lengths of the order of tens of fs or larger would resolve the double peak structure for the sequential process via the $Be^+(2p)$. The Fourier broadening of the sequential peaks for shorter pulses was demonstrated in helium [1]. The signature associated with the sequential ionization

via the $Be^+(2s)$, on the other hand, appears in the edges of the SDCS and is observed as "wings" in the SDCS in Fig. 2. Those wings are increasingly visible for the longest pulses plotted, 2 and 3 fs and are unapparent in shorter pulse lengths.

It is however noticeable that the signature for both sequential processes, central peak and wings, is only distinct for durations above 1 fs. One could then ask if the durations at which the peaks start to build up are associated with the time needed for the sequential ejection to take place (equivalently stated, to relaxation times for the ion after the sudden removal of an electron) or are they nothing more than the result of a spectral broadening effect.

A priori, an equivalent study for the helium atom would be the absorption of two 58 eV photons (energy right above the two-photon sequential threshold via the ground state of the ion). In that case, we observed that the sequential peaks started to show up at much shorter pulse lengths, T≃300 as [1]. However, for He the energy spacing between those sequential peaks is $E_0 - 2\epsilon_{n=1}(He^+) = 30$ eV and, therefore, we can not yet answer the question if the pulse length dependence is related at all to any time scale due to the sequential ejection itself or to spectral phenomena. We thus compute the SDCS for a higher photon energy, 24.8 eV, for which electrons are ejected with a larger energy gap. Fig. 3 shows the SDCS for pulses with different lengths, all centered at $\hbar\omega = 24.8$ eV, and leaving the outgoing electrons with an excess total energy of $E = 22.2$ eV to share. The features of sequential ionization associated with the $Be^+(2p)$ and $Be^+(2s)$ intermediate states, both located nearer to equal energy sharing appear more prominent at shorter pulse lengths compared to the previous example, as the spectral bandwidth of the pulses becomes less encompassing of the total excess energy available to share. In other words, the smaller energy gap between the ejected electrons is the only reason why longer pulse durations are required in Be than in He in order to uncover the sequential peaks for the double ionization of the valence electrons.

In Fig. 3, we also observe that for this higher photon energy new pathways for sequential ionization, via the intermediate cation now leaving the bound electron in $Be^+(n = 3)$ (levels also plotted in Fig. 1) are accessible to be populated by the first photon. The signature of this excitation ionization process becomes slightly observable in the extreme energy sharing wings of the 3.0 fs pulse of Fig. 3. This contribution, from the sequential processes through higher ionization thresholds, is noticeably lower than the signatures for the double ionization via the $Be^+(2p)$ and $Be^+(2s)$.

A similar trend was found for helium atom, but for the fact that it was only the sequential channel involving the ground state $He^+(1s)$ the one that is around two orders of magnitude more intense than sequential double ionization through excitation ionization. In the present work, we see that the relative magnitude of the first two

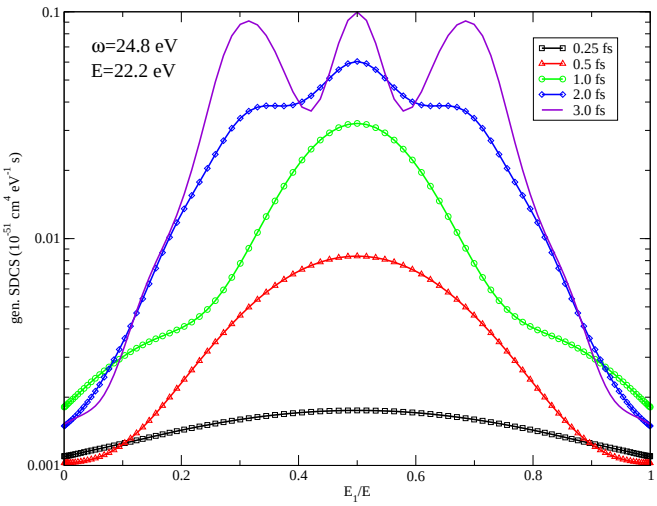

FIG. 3: (Color online) Same as Fig. 2, but with $\hbar\omega = 24.8$ eV photons. The excess energy above the double ionization threshold is $E = 22.2$ eV.

pairs of peaks are actually comparable, regardless the photon energy investigated. As the contributions of those energetically distant correlating configurations diminish in relative importance, we expect more disparate ratios in the relative sequential peak heights.

At this point, in order to elucidate how independent each photoejection is for the different sequential processes of beryllium, we consider a simple model employed in previous works [1, 7] for the sequential process in helium. Briefly, the amplitude for a two-photon transition is simplified from the formal time-dependent perturbation theory expression by assuming an *uncorrelated* final state symmetrized product of Coulomb waves and approximating the intermediate state as a the product of a bound state of the singly-ionized target and Coulomb function of the residual singly-charged ion. A full derivation of the model can be found in Ref. [1], but the relevant key finding from employing this model is that the features of the energy sharing cross section can be predicted for the lowest accessible sequential peaks of helium with surprising quantitative accuracy compared to the full calculation. Adapting this sequential framework, the SDCS for beryllium can be modeled as:

$$\frac{d\sigma^{\rm seq}(T)}{dE_1} \approx \left(\frac{32}{T}\right)^2 \frac{1}{4\pi\hbar} \Big| \sqrt{\sigma_{2p}^{\rm Be^+}(E_2)\sigma_{2p}^{\rm Be}(E_1)}\, G(\alpha_{1,2p}, T) + \sqrt{\sigma_{2p}^{\rm Be^+}(E_1)\sigma_{2p}^{\rm Be}(E_2)}\, G(\alpha_{2,2p}, T) + \sqrt{\sigma_{2s}^{\rm Be^+}(E_2)\sigma_{2s}^{\rm Be}(E_1)}\, G(\alpha_{1,2s}, T) + \sqrt{\sigma_{2s}^{\rm Be^+}(E_1)\sigma_{2s}^{\rm Be}(E_2)}\, G(\alpha_{2,2s}, T) \Big|^2 , \quad (16)$$

where $G(\alpha_{i,n}T)$ is the result of taking the rotating wave approximation and integrating the interacting field over

time,

$$G(\alpha,T)=\frac{1}{2}\int_0^T dt' e^{i\alpha t'}F(t)\times\frac{1}{2}\int_0^{t'} dt'' e^{-i\alpha t''}F(t) \tag{17}$$

and has a simple analytical form for sine-squared envelopes, $G(t)=\sin^2(\pi t/T)$. The excess energy terms are given by $\alpha_{i,n}=(E_0+\hbar\omega-E_i-\epsilon_n)/\hbar$ for the energy of either outgoing electron E_i and the ionization threshold energy ($n=2s$ or $2p$). Also, $\sigma^{\rm Be}(E_i)$ and $\sigma^{\rm Be^+}(E_i)$ refer to the single-photon photoionization cross sections of beryllium or beryllium cation, respectively, with intermediate states of $\rm Be^+(2s)$ or $\rm Be^+(2p)$. Each distinct photoionization amplitude is being approximated as the modulus square-root of the corresponding one-photon cross section, and it includes four terms total: a pair of direct and exchange terms for each of the $2p$ and $2s$ intermediate states of the Be cation, respectively.

This is a pure sequential model where we are neglecting any correlation in the intermediate or final states. In Fig. 4, we show the comparison of the model output (dashed curves) with the full calculation (solid curves) for 24.8 eV photons at the three longest pulse lengths previously considered. The model does predict the profiles for the SDCS with good agreement compared to the *ab initio* data for the position of the peaks and of the valleys resulting from the interference between terms coming from the 2s and from the 2p transitions in Eq. 16. It should be mention that the model presents a less quantitative consistency as the pulse length increases than comparisons carried out for helium. For Be, the model substantially underestimates the signal for the outer pair of sequential peaks, which is most likely due to the absence of the phase information between the individual photoionization events considered in this simple model, which is sacrificed by the approximation of these amplitudes backwards from their computed cross section values. This limitation is also suspected of slightly shifting the model peak locations of the secondary peaks relative to their anticipated values dictated by energy conservation. Despite the simplicity of the model, however, the general features of the energy sharing cross section and their behavior as the pulse length is increased are fairly well represented.

In the following, we examine the angular distributions for two-photon absorption. In contrast with helium, we already expect to gain an insight into a unique sequential process for the angular distributions near the sequential peaks around equal energy sharing: for electrons ejected with the same energy correlation effects would seem to be most important but, given the energetics of Be, electrons close to 50% energy sharing can be now ejected via a sequential process where mostly independent photon absorptions produce the final state electrons, and therefore less correlated between them might be expected. On the other hand, for unequal energy sharing, and taking into account the previous observations for helium, one can anticipate that close to the sequential peaks structures we will find more correlated angular distributions in Be than in He, due to the population of different principal partial waves by each photon compared to the dominant s to p transitions of each photoabsorption that describes the helium angular distributions well at its sequential peaks.

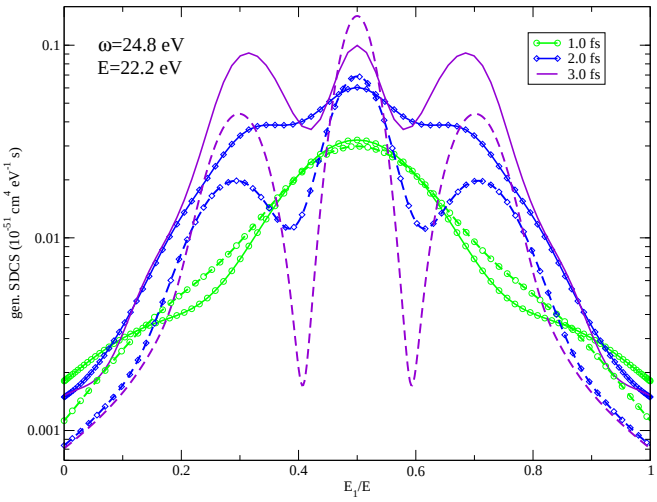

FIG. 4: Longer pulse duration results of Fig. 3 with $\hbar\omega=24.8$ eV photons (solid curves) along with sequential model results from Eq. 16 (dashed curves).

B. Angular distributions

We turn our attention to the (generalized) triply differential cross sections for two-photon double ionization of beryllium. For better comparison, we present the results normalized to their largest magnitude for each energy sharing, recalling that the double ionization amplitudes increase without bound as the pulse duration is lengthened. We examine the relative angular distributions at energy sharings of 30%, 50% and 90%, recalling that for the two photon central frequencies previously considered, 18.2 and 24.8 eV, a sequential peak is always placed near to one of these energy sharings.

Fig. 5 presents the angular distribution for double ionization with two photons of energy 18.2 eV. The second electron is plotted in the plane containing the first fixed electron directed along the polarization direction (taken to be the horizontal axis in the following figures). The fixed electron carries away the energy sharing indicated in each panel of the total $E=9.0$ eV excess energy available. The pulse lengths in each panel range from 0.5 fs to 3.0 fs. Firstly, examination of the unequal energy sharing panels, 30 and 90%, reveals a feature already exhibited in helium: for the longer pulses, the secondary peaks nearer to the fixed electron direction become more prominent, providing evidence of a time scale where the second outgoing electron becomes less sensitive to the direction of the first electron. In each energy sharing case, shorter pulse lengths lead to more back-to-back dominance in the

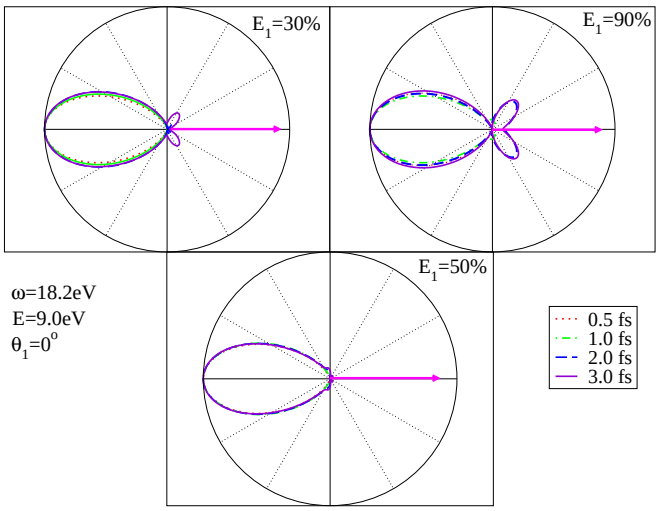

FIG. 5: (Color online) Angular distributions the second electron (θ_2) of Be double ionization at 18.2 eV photons in the plane containing the polarization direction (horizontal) and the fixed electron along the polarization ($\theta_1 = 0°$) carrying the energy sharing indicated in each panel. Results have been normalized to the largest magnitude cross section of the different pulse lengths for each energy sharing. The radius of each circle (in units of 10^{-54} cm^4 s eV^{-1} sr^{-2}) are 17 at 30%, 47 at 50%, and 14 at 90%.

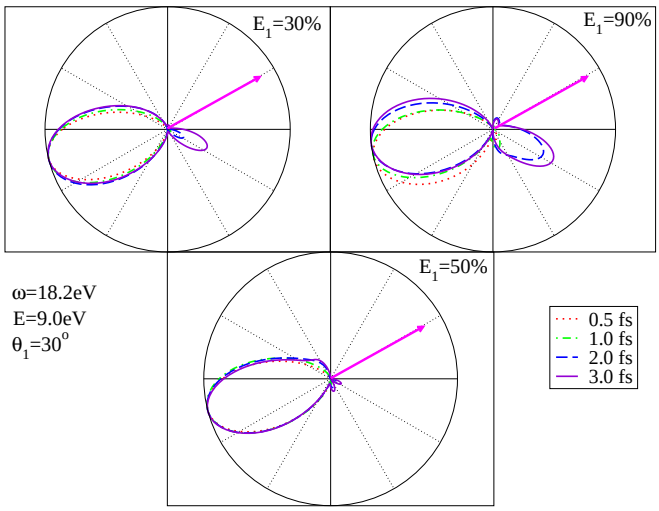

FIG. 6: (Color online) Same as Fig. 5, with the fixed electron electron now directed at $\theta_1 = 30°$ relative to the polarization direction. The radius of each circle (in units of 10^{-54} cm^4 s eV^{-1} sr^{-2}) are 11 at 30%, 47 at 50%, and 10 at 90%.

plotted electron angular distribution [1]. In other words, while both processes, sequential and direct two-photon ionization are open, the shorter the pulse, the larger the relative contribution of the direct process. The panel containing 90% energy sharing lying close to sequential ionization peak via the Be$^+(2s)$ intermediate shows the most change for longer pulses, as was demonstrated for the analogous intermediate pathway process in helium.

For 50% energy sharing, we expect to be catching the broadened sequential peaks via excitation ionization. This is qualitatively distinct from He, where at equal energy sharing direct two-photon ionization dominates. In the present case, we thus expect an uncorrelated angular distribution, i.e. a product of two independent s to p transitions. However, the result at equal energy sharing in the lower panel of Fig. 5 appears to be dominated by back-to-back ejection regardless of the pulse length, and exhibits no signature of sequential ionization previously seen for helium, despite the fact that the dominant sequential peak via the Be$^+(2p)$ intermediate lies on either side of this energy sharing midpoint less than 0.5 eV away. This distinction from sequential processes in helium is believed to be related to the larger energy separation between the sequential peaks from each other, and from equal energy sharing. By comparison, the behavior of the helium energy sharing cross section region near equal energy sharing has been viewed as the non-sequential background upon which the sequential peaks appear at their respective energies well separated from the energy sharing midpoint. This non-sequential background region shows relative little enhancement in helium as the pulse length increases, in contrast to the sequential peaks which exhibit a growing singular nature as the pulse duration becomes longer. The magnitude of the TDCS at 50% energy sharing does show the expected enhancement for the sequential process evident in the SDCS of Fig. 2. The radius of the equal energy sharing panel in Fig. 5 is nearly three times larger than the other energy sharing cases shown. Despite this increased magnitude indicating the proximity to a sequential enhancement, the angular distribution appears mostly non-sequential and correlated in the vicinity of the sequential peaks near equal energy sharing. Fig. 6 illustrates the same behavior for this photon energy with a different direction of the fixed electron, now aimed at $\theta_1 = 30°$ from the polarization direction. As before, more modification of the angular distribution is evident at unequal energy sharing as the pulse length is increased, the largest change occurring again at 90% energy sharing near the helium-like sequential peak. At $E_1/E = 50\%$ in the lower panel, the angular distribution again appears dominated by the correlated dynamics of equal energy sharing and much less sensitive to the pulse duration as compared to the asymmetric energy sharings. Again, the signature of this sequential process is an increase in the magnitude of the cross section by a factor of over 4 compared to the 30% and 90% panels of Fig. 6. The unique case of a sequential process enhancement that produces angular distributions that appear much more correlated as a consequence of lying near equal energy sharing truly distinguishes two-photon ionization of beryllium from helium.

Examining the angular distributions at the higher photon energy $\hbar\omega = 24.8$ eV corresponding to the SDCS of Fig. 3 further illustrates the distinct consequences of the location of the sequential peaks near or far from equal

energy sharing. Fig. 7 and Fig. 8 display the two-photon cross section at the higher photon energy for the same energy sharing percentages as presented above, and for the same fixed electron direction relative to the polarization, respectively. These results indicate again that for the large sequential peaks at 30% energy sharing via the $Be^+(2s)$ intermediate, the relative angular distributions are more sensitive to the pulse length. Since the symmetry of this transition is helium-like, a similar enhancement of the cross section with pulse duration is observed. This was previously modeled simply as the product of two dipole terms using the same unscreened independent-particle final state approximation used to derive Eq. 16. The predicted behavior of this product of s to p transitions is

$$\frac{d\sigma^{\rm seq}(T)}{dE_1 d\Omega_1 d\Omega_2} \approx \left(\frac{32}{T}\right)^2 \frac{1}{4\pi\hbar}\left(\frac{3}{4\pi}\right)^2 \cos^2(\theta_1)\cos^2(\theta_2) \times \left|\sqrt{\sigma^{\rm He^+}(E_2)\sigma^{\rm He}(E_1)}G(\alpha_1,T) + \sqrt{\sigma^{\rm He^+}(E_1)\sigma^{\rm He}(E_2)}G(\alpha_2,T)\right|^2, \quad (18)$$

and for the primary sequential peaks in helium illustrates the same behavior with pulse length seen in Fig. 7 at 30% energy sharing where the sequential peak in beryllium is similar in its intermediate channel. This behavior is also observed at 90% energy sharing for beryllium, but features an enhancement more favoring the ejected electron direction along the polarization for longer pulses, where again, interference terms between the $Be^+(n=3)$ not accounted for in the expanded simple model analogous to Eq. 18 are unaccounted for, but whose overall shape for longer pulses demonstrates the same behavior. However, the TDCS is substantially smaller in magnitude compared to the less extreme energy sharings, owing to this process again representing an excitation-ionization to higher principal $n = 3$ state of the intermediate cation. The unequal energy sharing upper panels of Fig. 8 in particular also provide a slight contrast to the helium case where the importance of higher angular momentum terms that contribute more strongly for beryllium than for helium sequential ionization convergence result in slightly more distorted lobes than the simple product-dipole patters of helium for this photoejection direction.

As was the case for the lower photon energy considered, it is the overlapping sequential peaks near equal energy sharing that show an enhancement in the magnitude of the generalized cross section but demonstrate a correlated back-to-back angular distribution in Fig. 7 and Fig. 8 at even the longer pulse durations considered. Again, the energetic symmetry of the exiting electrons produces angular patterns that appear highly correlated and insensitive to the pulse duration, indicating that the consequence of the sequential ionization producing photoelectrons with nearly the same kinetic energy renders an independent particle model unable to accurately represent what final-state correlation requires when the electrons move with nearly the same kinetic energy in the continuum. The resulting angular distributions in these cases appear to bear the signature of direct ionization sensitive to correlation in the final state rather than sequential ionizations which leave the electrons energetically distinct, as in the upper panels of Fig. 7 and Fig. 8.

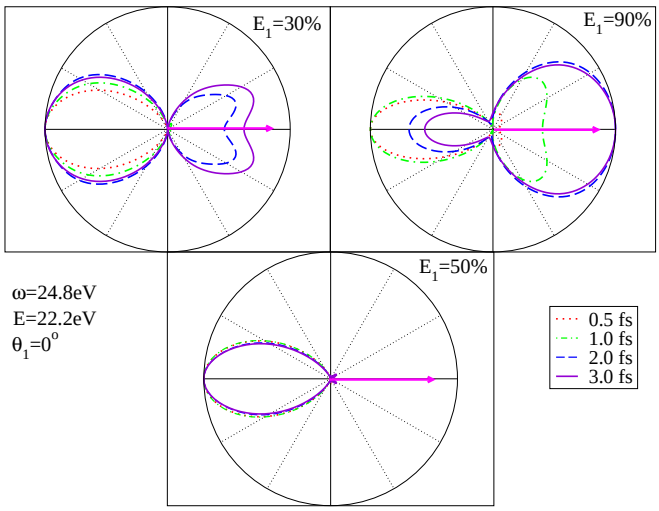

FIG. 7: (Color online) Same as Fig. 5, for double ionization with 24.8 eV photons with the fixed electron electron directed at $\theta_1 = 0^\circ$ relative to the polarization direction. The radius of each circle (in units of 10^{-55} cm^4 s eV^{-1} sr^{-2}) are 45 at 30%, 200 at 50%, and 2 at 90%.

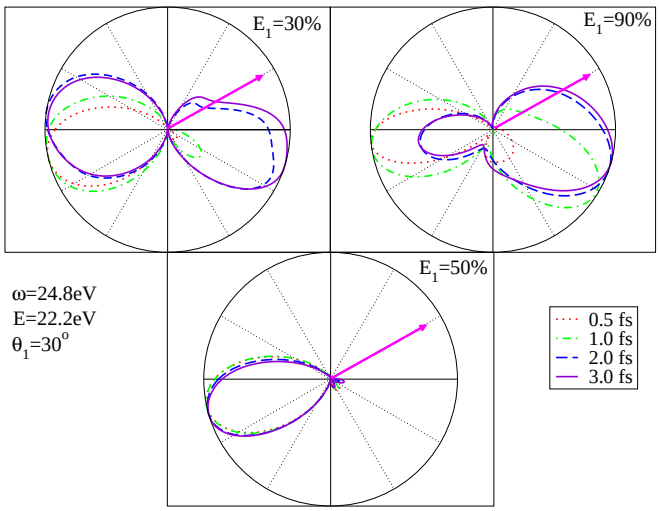

FIG. 8: (Color online) Same as Fig. 7, with the fixed electron electron now directed at $\theta_1 = 30^\circ$ relative to the polarization direction. The radius of each circle (in units of 10^{-55} cm^4 s eV^{-1} sr^{-2}) are 34 at 30%, 140 at 50%, and 1.6 at 90%.

IV. CONCLUSION

We have presented energy and angle-differential theoretical results for double ionization of the valence electrons of beryllium by two-photon absorption. The symmetry of the problem in beryllium bears much in common with helium, but we have found substantial differences in the behavior of the double ionization amplitudes for sequential ionization via the first sequential threshold. This is due to the mechanism proceeding via the first excited state of the intermediate of the excited-state cation $Be^+(2p)$, which bears less similarity to the ground state intermediate $He^+(1s)$ encountered in helium sequential ionization. Further, in beryllium the energetics of the process require that a sequential two-photon ionization via this intermediate produces photoelectrons with outgoing kinetic energies separated by less than 1 eV, and thus highly correlated in energy sharing. The consequences of this imply that an independent particle model to describe the angular distributions does not fully capture the final-state dynamics that produces predominantly back-to-back photoejection patterns reminiscent of correlated processes such as single-photon double ionization and non-sequential two-photon double ionization. This is in stark contrast to helium where the sequential process can be very well modeled by viewing the two-photon absorption at the sequential peaks as the product of two independent photoionization events because the continuum electrons are well-separated in energy.

Though the first sequential threshold in beryllium is distinct compared to helium in the intermediate cation produced after the first photoabsorption, at slightly higher photon energies the analogous process via the ground state intermediate $Be^+(2s)$ opens, resulting in a second pair of sequential peaks whose energy separation is larger, and therefore less correlated in the final state. Examination of the angular distributions corresponding to this sequential process reveals much more commonality with the behavior of helium in two-photon ionization at the sequential peak energy sharings. There, the process of ionization does appear to be much better modeled by two independent photoionization events as in Eq. 18.

The simple uncorrelated final state model employed that better describes the helium-like transitions producing energetically distinct photoelectrons in two-photon absorption also hints at the limitations that arise from ignoring the interference terms between two competing sequential ionization pathways, as evidenced in the energy-sharing cross section of Fig. 4. While the model does successfully predict the location and bandwidth-limited spectral resolution of the sequential peaks fairly well, for longer duration pulses this approximation qualitatively underestimates the double ionization amplitude between the central and helium-like sequential peaks and is much less quantitatively accurate at describing the relative peak heights than when applied to the simpler helium atom. As the beryllium atom features substantially more important contributions from the lower few correlating configurations than does helium, the phase information between sequential pathways must seemingly be more important to retain in order to better model the *ab initio* results.

[1] A. Palacios, T. N. Rescigno, and C. W. McCurdy, Phys. Rev. A **79**, 033402 (2009).

[2] M. F. Kling and M. J. J. Vrakking, Annual review of physical chemistry **59**, 463 (2008), ISSN 0066-426X, URL http://www.ncbi.nlm.nih.gov/pubmed/18031218.

[3] K. Midorikawa, Japanese Journal of Applied Physics **50**, 090001 (2011), ISSN 0021-4922, URL http://stacks.iop.org/1347-4065/50/090001.

[4] L. Gallmann, C. Cirelli, and U. Keller, Annual review of physical chemistry **63**, 447 (2012), ISSN 1545-1593, URL http://www.ncbi.nlm.nih.gov/pubmed/22404594.

[5] C. Bostedt, H. N. Chapman, J. T. Costello, J. R. Crespo López-Urrutia, S. Düsterer, S. W. Epp, J. Feldhaus, A. Föhlisch, M. Meyer, and T. Möller, Nuclear Instruments and Methods in Physics Research Section A: Accelerators, Spectrometers, Detectors and Associated Equipment **601**, 108 (2009), ISSN 01689002, URL http://linkinghub.elsevier.com/retrieve/pii/S0168900208023201.

[6] J. Ullrich, A. Rudenko, and R. Moshammer, Annual review of physical chemistry **63**, 635 (2012), ISSN 1545-1593, URL http://www.ncbi.nlm.nih.gov/pubmed/22404584.

[7] A. Palacios, D. A. Horner, T. N. Rescigno, and C. W. McCurdy, Journal of Physics B: Atomic, Molecular and Optical Physics **43**, 194003 (2010).

[8] a. a. Sorokin, M. Wellhöfer, S. V. Bobashev, K. Tiedtke, and M. Richter, Physical Review A **75**, 051402 (2007), ISSN 1050-2947, URL http://link.aps.org/doi/10.1103/PhysRevA.75.051402.

[9] H. Hasegawa, E. J. Takahashi, Y. Nabekawa, K. L. Ishikawa, and K. Midorikawa, Physical Review A **71**, 023407 (2005), ISSN 1050-2947, URL http://link.aps.org/doi/10.1103/PhysRevA.71.023407.

[10] P. Antoine, E. Foumouo, and B. Piraux, Physical Review A **78**, 1 (2008), ISSN 1050-2947, URL http://link.aps.org/doi/10.1103/PhysRevA.78.023415.

[11] M. W. McIntyre, a. J. Kinnen, and M. P. Scott, Physical Review A **88**, 053413 (2013), ISSN 1050-2947, URL http://link.aps.org/doi/10.1103/PhysRevA.88.053413.

[12] M. S. Pindzola, C. P. Ballance, S. a. Abdel-Naby, F. Robicheaux, G. S. J. Armstrong, and J. Colgan, Journal of Physics B: Atomic, Molecular and Optical Physics **46**, 035201 (2013), ISSN 0953-4075.

[13] D. Griffin, M. Pindzola, C. Ballance, and J. Colgan, Physical Review A **79**, 023413 (2009), ISSN 1050-2947, URL http://link.aps.org/doi/10.1103/PhysRevA.79.023413.

[14] S. Laulan and H. Bachau, Phys. Rev. A **69**, 033408 (2004).

[15] M. Kurka, a. Rudenko, L. Foucar, K. U. Kühnel,

Y. H. Jiang, T. Ergler, T. Havermeier, M. Smolarski, S. Schössler, K. Cole, et al., Journal of Physics B: Atomic, Molecular and Optical Physics **42**, 141002 (2009), ISSN 0953-4075, URL http://stacks.iop.org/0953-4075/42/i=14/a=141002?key=crossref.29c58c23c9188bdd1f4cfab2d10a9793.

[16] E. Benis, D. Charalambidis, T. Kitsopoulos, G. Tsakiris, and P. Tzallas, Physical Review A **74**, 051402 (2006), ISSN 1050-2947, URL http://link.aps.org/doi/10.1103/PhysRevA.74.051402.

[17] P. Tzallas, E. Skantzakis, L. a. a. Nikolopoulos, G. D. Tsakiris, and D. Charalambidis, Nature Physics **7**, 781 (2011), ISSN 1745-2473, URL http://www.nature.com/doifinder/10.1038/nphys2033.

[18] F. L. Yip, C. W. McCurdy, and T. N. Rescigno, Phys. Rev. A **81**, 053407 (2010).

[19] F. L. Yip, C. W. McCurdy, and T. N. Rescigno, Phys. Rev. A **81**, 063419 (2010).

[20] A. Palacios, C. W. McCurdy, and T. N. Rescigno, Phys. Rev. A **76**, 043420 (2007).

[21] A. Palacios, T. N. Rescigno, and C. W. McCurdy, Phys. Rev. A **77**, 032716 (2008).

[22] F. Yip, A. Palacios, T. Rescigno, C. McCurdy, and F. Martn, Chemical Physics **414**, 112 (2013).

[23] J. Colgan and M. Pindzola, Physical Review A **65**, 022709 (2002), ISSN 1050-2947, URL http://link.aps.org/doi/10.1103/PhysRevA.65.022709.

[24] T. N. Rescigno and C. W. McCurdy, Phys. Rev. A **62**, 032706 (2000).

[25] C. W. McCurdy, M. Baertschy, and T. N. Rescigno, J. Phys. B **37**, R137 (2004).

[26] T. N. Rescigno, M. Baertschy, and C. W. McCurdy, Phys. Rev. A **68**, 020701 (2003).

[27] E. Foumouo, G. L. Kamta, G. Edah, and B. Piraux, Phys. Rev. A **74**, 063409 (2006).

[28] V. Hernandez, J. E. Roman, and V. Vidal, ACM Trans. Math. Software **31**, 351 (2005).

[29] V. Hernandez, J. E. Roman, A. Tomas, and V. Vidal, Tech. Rep. STR-6, Universitat Politècnica de València (2009), available at http://www.grycap.upv.es/slepc.

[30] S. Balay, S. Abhyankar, M. F. Adams, J. Brown, P. Brune, K. Buschelman, V. Eijkhout, W. D. Gropp, D. Kaushik, M. G. Knepley, et al., *PETSc Web page*, http://www.mcs.anl.gov/petsc (2014), URL http://www.mcs.anl.gov/petsc.

[31] D. A. Horner, F. Morales, T. N. Rescigno, F. Martin, and C. W. McCurdy, Phys. Rev. A **76**, 030701 (2007).